RSC Advances

PAPER

View Article Online
View Journal | View Issue

Cite this: *RSC Adv.*, 2014, **4**, 42234

Three-dimensional hybridized carbon networks for high performance thermoelectric applications

Xiaojian Tan,[a] Hezhu Shao,[a] Yanwei Wen,[b] Huijun Liu[c] and Guoqiang Liu*[a]

Received 24th June 2014
Accepted 2nd September 2014

DOI: 10.1039/c4ra06149g

www.rsc.org/advances

Thermoelectric properties of three-dimensional covalently connected carbon networks are investigated by using first-principles calculation, Boltzmann transport theory, and nonequilibrium molecular dynamics simulations. It is found that the electronic transport of such networks exhibit "ballistic transport" behavior, similar to single carbon nanotubes. The thermoelectric performance of network structures is significantly enhanced relative to one-dimensional carbon nanotubes, owing to the high power factor and largely reduced thermal conductivity. The *ZT* value of carbon network (9,0) at intermediate temperature can be increased to 0.78 by n-type doping with a carrier concentration of 3.9×10^{19} cm^{-3}. Therefore carbon networks are expected to be potential candidates for eco-friendly thermoelectric materials.

1 Introduction

Thermoelectric materials are being paid a lot of research attention in the past decades because of their direct conversion between heat and electricity. Due to the exhaustion of fossil fuels and the related environmental problems, it is urgently needed to develop eco-friendly and high performance thermoelectric devices. The efficiency of a thermoelectric material is quantified by the dimensionless figure of merit $ZT = S^2\sigma T/(\kappa_e + \kappa_{ph})$, where S is the Seebeck coefficient, σ is the electrical conductivity, T is the absolute temperature, and κ is the thermal conductivity that contains both the electronic (κ_e) and lattice components (κ_{ph}). An ideal thermoelectric material is described as "phonon glass electron crystal (PGEC)", *i.e.*, a high *ZT* value material should have high S, high σ, and low $\kappa = \kappa_e + \kappa_{ph}$.[1] Such a task is usually difficult to achieve since there is a strong correlation of S, σ, and κ_e according to the Wiedemann–Franz law.[2] Considering the relative weak correlation between κ_{ph} and the other coefficients, an effective way to improve the *ZT* values of thermoelectric materials is reducing the thermal conductivity while keeping the electronic transport less affected.

Carbon nanotubes (CNTs) have attracted much research interest as an ideal candidate for building new types of electronic devices because of their exceptional electronic transport properties. Compared with the conventional thermoelectric materials, carbon materials are environmentally friendly and easy for mass produce. Unfortunately, the thermal conductivity of CNTs is as high as thousands of W m^{-1} K^{-1},[3–6] owing to the long phonon mean free path and large group velocity.[7] The theoretically predicated *ZT* value of tube (10,0) is only 0.2 at 300 K.[8] Recently, CNT bulk samples[9] and three-dimensional CNT structures[10,11] have been prepared and their thermal conductivities are found to be significantly reduced to 0.035–4.2 W m^{-1} K^{-1} due to the strong tube–tube interaction. However, the reported power factor $S^2\sigma$ of such CNT bulk materials[10–12] and nanocomposites[13] vary in the range of 2.2–25 μW m^{-1} K^{-2}, and the measured electrical conductivities are orders of magnitude lower than those of individual CNTs, resulting in very lower *ZT* values of 0.002–0.2. The poor power factor and thermoelectric properties in CNT bulk materials are due to the coiled and randomly oriented structures produced in the fabrication process. It is conceivable that the periodically assembled CNT bulk materials may exhibit significantly decreased thermal conductivity whereas the electronic properties are less affected. Very recently, a new type of carbon bulk materials composed with three-dimensional covalently connected carbon network have been reported to be more thermodynamically stable structures with low kinetic barrier of formation.[14] These networks are long range ordered CNTs connected by strong covalent C–C bonds, which are very different from the previously reported CNT bulk materials. To be distinguished with the CNT bulk materials composed of coiled and randomly oriented CNTs, these ordered and covalently connected CNT bulk materials are called as sp^2–sp^3 hybridized carbon networks (HCNs).[14] It is interesting to explore their possible application as thermoelectric materials.

In this work, the electronic and phonon transport properties of HCNs are investigated by using the semiclassical Boltzmann theory and nonequilibrium molecular dynamics (NEMD)

[a]*Ningbo Institute of Materials Technology and Engineering, Chinese Academy of Science, Ningbo 315201, China. E-mail: liugq@nimte.ac.cn; Fax: +86-574-86688067; Tel: +86-574-86688067*

[b]*Department of Materials Science and Engineering, Huazhong University of Science and Technology, Wuhan 430074, China*

[c]*Key Laboratory of Artificial Micro- and Nano-structures of Ministry of Education and School of Physics and Technology, Wuhan University, Wuhan 430072, China*

simulations respectively. We shall show that the electronic properties of such three-dimensional ordered HCNs are some lower or close to those of one-dimensional CNTs, but much higher than those of the coiled and randomly oriented CNT bulk materials. Considering the significantly reduced thermal conductivity, these HCNs could exhibit relatively large power factor and high thermoelectric performance by appropriate p-type and n-type doping.

2 Computational details

The structure optimization and energy band-structure calculations of HCNs are performed using a plane-wave pseudopotential formulation[15–17] within the framework of density functional theory (DFT). The exchange–correlation energy is in the form of Perdew–Burke–Ernzerhof (PBE)[18] using generalized gradient approximation (GGA). Projector-augmented wave (PAW) potentials are used for the carbon atoms and the cutoff energy is set as 400 eV. During the geometry optimizations, both the atoms positions and lattice constants are fully relaxed until the magnitude of the force acting the atoms is less than 0.01 eV Å^{-1}, which also converge the total energy within 1 meV. The Brillouin zone is sampled with 10 × 10 × 20 Monkhorst–Pack k-meshes.

The transport properties were calculated from the electronic structure using a semiclassical approach by solving the Boltzmann's equation as implemented in the BoltzTraP code[19] within the constant relaxation time approximation, which has been successfully applied to a wide range of thermoelectric materials.[20] The kernel is to find the so-called transport distribution, which can be expressed as:

$$\Xi = \sum_{\vec{k}} \vec{v}_{\vec{k}} \vec{v}_{\vec{k}} \vec{\tau}_{\vec{k}}, \quad (1)$$

where $\vec{v}_{\vec{k}}$ and $\vec{\tau}_{\vec{k}}$ is the group velocity and relaxation time at state $\vec{k}$, respectively. The electrical conductivity σ, Seebeck coefficients S, and electronic thermal conductance κ_e can be calculated according to:

$$\sigma = e^2 \int d\varepsilon \left(-\frac{\partial f_0}{\partial \varepsilon} \right) \Xi(\varepsilon), \quad (2)$$

$$S = \frac{e k_B}{\sigma} \int d\varepsilon \left(-\frac{\partial f_0}{\partial \varepsilon} \right) \Xi(\varepsilon) \frac{\varepsilon - \mu}{k_B T}, \quad (3)$$

$$\kappa_e = {k_B}^2 T \int d\varepsilon \left(-\frac{\partial f_0}{\partial \varepsilon} \right) \Xi(\varepsilon) \left(\frac{\varepsilon - \mu}{k_B T} \right)^2, \quad (4)$$

where f_0 is the equilibrium Fermi function, k_B is the Boltzmann's constant, and μ is the chemical potential.

Other than above quantities, the lattice thermal conductivity κ_{ph} is predicted based on the Fourier's law where the heat flow and temperature profile are realized using the NEMD simulations as implemented in the LAMMPS code.[21] The Tersoff[22] potential is adopted to describe the inter-atomic interactions and the time step is fixed as 0.5 fs. We carry out a 300 ps constant temperature simulation and a 200 ps constant energy simulation to ensure the system reaches a steady state. The HCNs are then divided into 40 equal segments along the direction of heat flow with periodic boundary conditions, where the cold and hot regions are located at 1st and 21st segment, respectively. The hottest atoms in the cold region and the coldest ones in the hot region swap their kinetic energies according to the Müller-Plathe algorithm,[23] then the temperature gradient responses and thermal flux maintains by atoms' interactions in neighboring segments.

3 Results and discussion

The structures of HCNs have already been reported in ref. 14, and they can be visualized as self-assembled one-dimensional CNTs of small diameter. In HCNs, the CNTs first rearrange into triplet structures and then form a three-dimensional network by joining the reactive tips. CNTs can be specified by a pair of integers (n,m), corresponding to a chiral vector $C_h = na_1 + ma_2$, where a_1 and a_2 are the graphene lattice vectors. In this work, we also use this nomenclature for HCNs. Fig. 1 is the top view of four kinds of HCNs: (5,0), (6,0), (8,0), and (9,0), which are made up of the (5,0), (6,0), (8,0) and (9,0) tubes, respectively. All of these HCNs have a hexagonal lattice, and their lattice constants (a and c) are indicted in Fig. 1(a). The primitive cell of each contains 60, 72, 96, and 108 carbon atoms, indicated by shadow in Fig. 1. As summarized in Table 1, the lattice constant c is almost 4.24 Å for all of four HCNs while a is almost linearly increased from 12.84 to 20.34 Å. This is easy to be understood because CNTs (5,0), (6,0), (8,0), and (9,0) have the same cell length but different tube diameters.

Fig. 2(a)–(d) show the calculated band structures of four kinds of HCNs. Our first principle calculations indicate that these HCNs are all semiconductors and the band gaps are 0.14, 1.21, 0.50, and 1.01 eV as listed in Table 1. HCN (7,0) is found to be metallic in our calculation, and then it is not suitable for thermoelectric application. We will not discuss the transport properties of HCN (7,0) in this work. In the Brillouin zone, the bands obviously disperse along the directions parallel to c axis such as "K–H, L–M, and Γ–A", while they are almost dispersionless along the directions vertical to c axis such as "Γ–K,

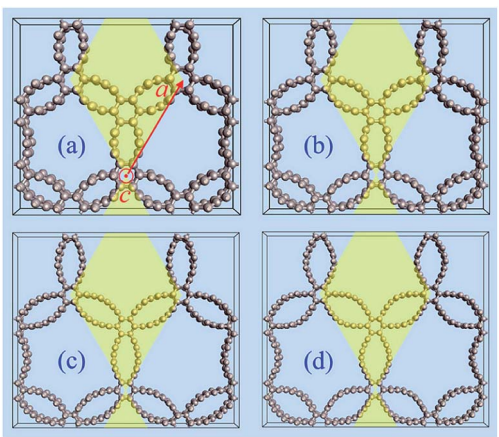

Fig. 1 (Color online) Top view of four kinds of HCNs: (a) (5,0), (b) (6,0), (c) (8,0), and (9,0). The primitive cells are shaded.

Table 1 Lattice constant a and c, and band gap E_g for four kinds of HCNs: (5,0), (6,0), (8,0) and (9,0)

Structure	a (Å)	c (Å)	E_g (eV)
HCN (5,0)	12.84	4.22	0.14
HCN (6,0)	14.88	4.23	1.21
HCN (8,0)	18.81	4.24	0.50
HCN (9,0)	20.34	4.24	1.01

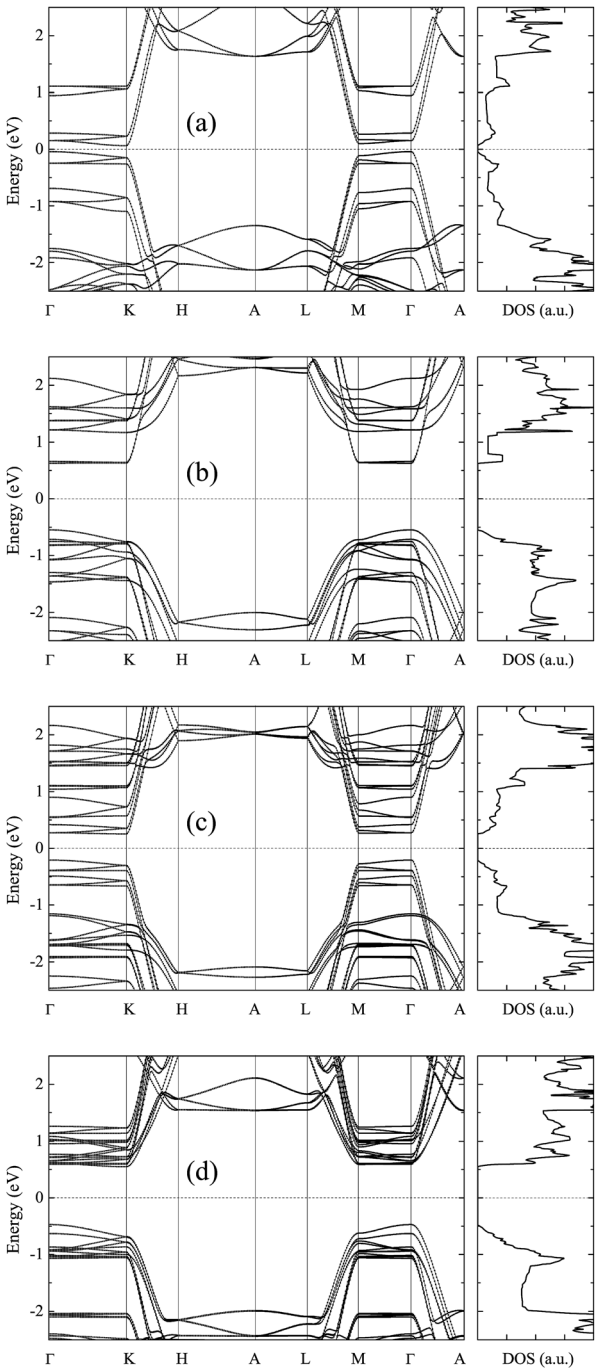

Fig. 2 Calculated energy band structures and density of state (DOS) for (a) (5,0), (b) (6,0), (c) (8,0), and (d) (9,0) HCNs, the dash line indicates the Fermi level.

H–A–L, and *M–Γ*". As may be seem in Fig. 2, three-dimensional HCNs roughly keep the quasi-one-dimensional electronic transport behavior of single CNTs. As known, the electrons in CNTs exhibit "ballistic transport" behavior, thus it is reasonable to expect the good electronic transport properties of HCNs. The abrupt band structures parallel to c axis indicate high carrier mobility and high electrical conductivity, and the flat bands vertical to c axis result in the DOS peaks and high Seebeck coefficient at the edge of band gap.[1,24] As shown in Fig. 2(d), HCN (9,0) exhibits sharp DOS peaks at the bottom of conduction bands, leading to a high absolute value of the n-type Seebeck coefficient at the optimized doping level ($\sim 10^{20}$ cm^{-3}).

The electronic transport coefficients of HCNs can be evaluated by using the Boltzmann theory and relaxation time approximation, based on the calculated band structures. In this approach, the Seebeck coefficient S is independent of the relaxation time τ, while the electrical conductivity, electronic thermal conductivity and power factor can only be determined with respect to the relaxation time. The coefficients we actually calculated are namely σ/τ, κ_e/τ, and $S^2\sigma/\tau$. To get reliable results, we use a very dense k mesh up to 1600 points in the BoltzTraP calculations. By integrating the calculated band structures in the irreducible BZ according to eqn (1)–(4), the electronic transport coefficient σ/τ, κ_e/τ, S and $S^2\sigma/\tau$ can be obtained.

Fig. 3 shows the corresponding transport coefficients of four kinds of HCNs at 300 K as a function of chemical potential μ, where the Fermi level is at $\mu = 0$ eV. Within the rigid band approximation,[25] the chemical potential μ indicates the doping level or carrier concentration of the system, and p-type doping corresponds to $\mu < 0$, while n-type doping corresponds to $\mu > 0$. As can be seen in Fig. 3(a) and (b), electrical conductivity σ/τ and electronic thermal conductivity κ_e/τ exhibit similar variation tendency with respect to chemical potential μ according to Wiedemann–Franz law. Both of them vanish around the Fermi level since this area corresponds to the band gap of system. When the chemical potential moves to the edge of the band gap, σ/τ and κ_e/τ exhibit an obvious increase as the increasing DOS (see Fig. 2).

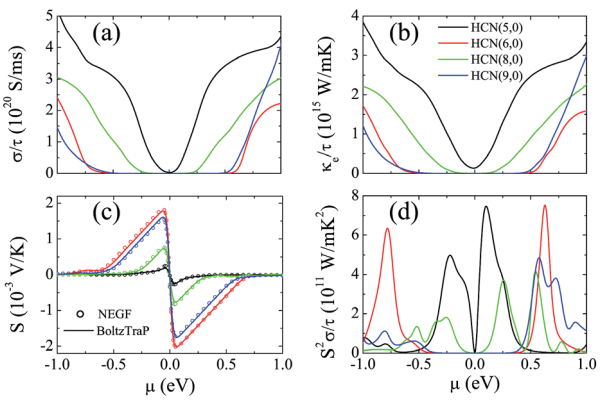

Fig. 3 (Color online) Calculated transport coefficients at 300 K as function of chemical potential μ for HCNs: (a) electrical conductivity σ/τ, (b) electronic thermal conductivity κ_e/τ, (c) Seebeck coefficient S, and (d) power factor $S^2\sigma/\tau$.

Fig. 3(c) shows the roughly antisymmetric structure of the Seebeck coefficient S. As the doping level moves from 0 to ±1 eV, the absolute value of S increases sharply near the Fermi level, reaches the maximum value at $\mu = \pm k_B T$, and then decreases to zero near the edge of the band gap. The maximum absolute value of S increases with the increasing band gap. With wider band gaps, HCNs (6,0) and (9,0) exhibit higher Seebeck coefficient S than HCNs (5,0) and (8,0). We also calculated the Seebeck coefficient using the nonequilibrium Green's function (NEGF) method as implemented in the ATK code, which is widely used to study the quantum transport properties of electrons.[26,27] The NEGF results are very consistent to the BoltzTraP results for all of these HCNs. As the NEGF method is only focus on the "ballistic transport", thus the electron transport behavior in HCNs is very close to "ballistic transport". It should be mentioned that the maximum of Seebeck coefficient is at a very low carrier concentration, and it is difficult to be achieved in experiment. A high Seebeck coefficient is not necessarily useful. For thermoelectric materials, it is more important to maximize the thermoelectric power factor.

As known, there is a tradeoff between the electrical conductivity σ and the Seebeck coefficient S, and one need to find a proper doping level to maximize the value of power factor $S^2\sigma/\tau$. When the doping level reaches the edge of the band gap, both σ/τ and S are nonzero, thus the power factor $S^2\sigma/\tau$ exhibits some peaks at the edge of the band gap (see Fig. 3(d)). Moreover, the corresponding electronic thermal conductance κ_e/τ is relatively low, which is also beneficial to achieve high thermoelectric performance.

In ref. 14, the thermo stability of HCNs has been discussed by using molecular dynamics simulations and the results indicate that formed HCNs remain stable under ambient temperatures and only transform back to regular CNT bundles at an elevated temperature of about 1400 K. Therefore these ordered network structures may be potential intermediate temperature thermoelectric materials. At a given doping level, chemical potential μ changes with the variation of temperature, we then consider the thermoelectric properties as a function of carrier concentration instead of chemical potential. The power factor $S^2\sigma/\tau$ map is plotted as a function of temperature T and carrier concentration n for these networks in Fig. 4, where $n > 0$ denotes n-type doping and $n < 0$ denotes p-type doping. As indicate in the color scale, the bright red and deep blue stand for large and small calculated values of $S^2\sigma/\tau$, respectively. It can be seen that the calculated power factor of these HCNs exhibit several highlight areas with obviously large values in a wide temperature range. HCNs (5,0) favors n-type doping and (6,0) favors p-type doping. In all these networks, n-type doped HCN (9,0) exhibits the highest power factor $S^2\sigma/\tau$ (1.94×10^{12} W m^{-1} K^{-2} s^{-1}) at 900 K with $n = 8.2 \times 10^{20}$ cm^{-3}, which is consistent with the above discussion about energy band structure and DOS.

Up to now, we have dealt with electronic transport properties of these HCNs. As discussed in the introduction part, formation of networks or bulk material can significantly reduce the lattice thermal conductivity κ_{ph} of CNTs to as low as several W m^{-1} K^{-1}.[9–11] In this work, the phonon derived thermal conductivity

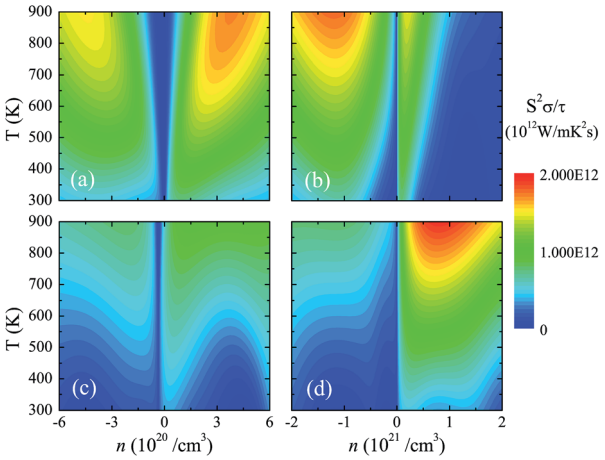

Fig. 4 (Color online) Calculated power factor $S^2\sigma/\tau$ map as a function of temperature T and carrier concentration n for (a) HCN (5,0), (b) HCN (6,0), HCN (8,0), and (d) HCN (9,0).

κ_{ph} of ordered HCNs is calculated according to the Fourier's law by using NEMD method. NEMD simulation can also handle nonlinearity when dealing with heat transport and has been shown to be an efficient way to calculate thermal conductivity, including both ballistic and diffusive transport, from room to intermediate temperature.[29] It is well-known that thermal conductivity of nanostructures is size-dependent[30] and it can be empirically fitted as the power law $\kappa_{ph} \sim l^{\alpha}$ ($0 < \alpha < 1$), where exponent α depends on the temperature and sample length l. We calculate the thermal conductivity at different sample lengths and then extrapolate to an infinite length according to the linear relationship between $1/\kappa_{ph}$ and $1/l$. Our calculated room temperature lattice thermal conductivity κ_{ph} of four kinds of networks are summarized in Fig. 5. The lattice thermal conductivity of the series decreases with the increasing temperature. A similar observation was also found in one-dimensional CNTs and can be attributed to the more frequent phonon umklapp scattering in the systems at higher temperature.[31] At a certain temperature, we find that the lattice thermal conductivity decreases as the lattice constant a is increased, which is similar to the case of one-dimensional CNTs, *i.e.*, CNTs

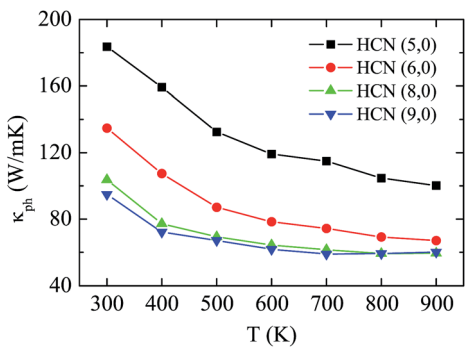

Fig. 5 (Color online) Calculated lattice thermal conductivity κ_{ph} of HCNs as a function of temperature T.

with larger diameter exhibit lower lattice thermal conductivity.[28,31] Compared with the previous reported results of single CNTs (usually thousands of W m^{-1} K^{-1}), κ_{ph} of these HCNs are almost one order of magnitude lower, which may be caused by the strong tube–tube interaction and increased phonon scattering modes.[9,10] On the other hand, κ_{ph} of these HCNs are much higher than those of the previous reported results of CNT bulk materials because of the much ordered structures. Anyhow, formation of HCNs can significantly reduce κ_{ph} of system as well as keeps the excellent electronic transport properties, and enhances their thermoelectric performance.

As discussed above, the power factor $S^2\sigma/\tau$ of n-type doped HCN (9,0) is nearly 2.0×10^{12} W m^{-1} K^{-2} s^{-1} at 900 K, and the lattice thermal conductivity κ_{ph} at 900 K is 60 W m^{-1} K^{-1}. With the highest power factor and the lowest thermal conductivity, HCN (9,0) is the most favorable thermoelectric candidate among these networks. To evaluate the *ZT* value explicitly, one need obtain the electron relaxation time τ. The accurate evaluation of τ depends on the detailed scattering mechanism and is usually estimated by fitting experimentally measured electrical conductivity or electron mean free path. Unfortunately, such experimental date is not available for such ordered network structures, and we use the electron mean free path $l_e = 1.5$ μm of semiconducting CNTs[32–35] as an alternative. This is a reliable approximation since the electronic transport character of HCNs is very similar to those of the single CNTs. For shorter CNTs, the electron transport is in the region of ballistic transport and the electrical conductance G_E can be obtained by using NEGF method; at longer length l, the electrical conductance G is reduced by scattering according to $G = G_E l_e/l$,[32] thus the electrical conductivity σ is converged to $G_E l_e/A$, where A is the cross area section. By using such a approach, the fitted relaxation time τ is in the range of 0.4–1.0 $\times$ 10^{-12} s for these ordered HCNs.

Fig. 6(a)–(d) show the two-dimensional maps of *ZT* (n, T) when the relaxation time τ is 0.4, 0.6, 0.8, and 1.0 $\times$ 10^{-12} s. By appropriate n-type doping with $n = 7.6 \times 10^{19}$ cm^{-3}, the optimized *ZT* value of HCN (9,0) is 0.43 at room temperature. The optimized *ZT* value of HCN (9,0) can be further increased with the increasing temperature. As τ in a range of 0.4–1.0 $\times$ 10^{-12} s, the maximum *ZT* value of ordered HCN (9,0) reaches 0.7–0.8 at 900 K with $n = 3.9 \times 10^{19}$ cm^{-3} by n-type doping. The obtained maximum *ZT* of 0.8 is much higher than the values of individual CNTs[8] or previous CNT bulk materials.[10–13] The lattice thermal conductivity κ_{ph} of HCNs is as high as 60 W m^{-1} K^{-1}, and there is still a large space to further reduce κ_{ph} and improve the *ZT* value with different means, such as isotope doping[36] and surface decoration.[37] Our calculations indicate that when one-dimensional nanotubes form covalently connected three-dimensional ordered HCNs, the electronic transport properties are less affected with the thermal conductivity significantly reduced, which leads to high thermoelectric performance.

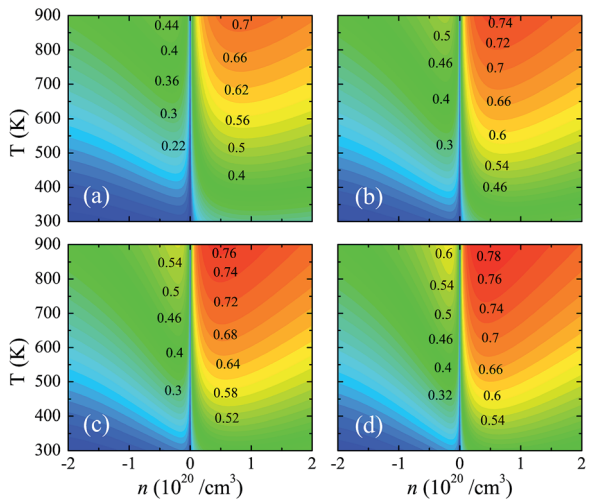

Fig. 6 (Color online) Calculated *ZT* value map of HCN (9,0) as a function of temperature T and carrier concentration n for relaxation time τ = (a) 0.4, (b) 0.6, (c) 0.8, and (d) 1.0 $\times$ 10^{-12} s.

4 Summary

In summary, we have studied the thermoelectric properties of four kinds of ordered carbon networks by using multiscale approach. The first-principles calculated band structures of HCNs indicate their electronic transport properties is similar to those of individual CNTs, and the sharp increased DOS leads to a high value of Seebeck coefficient. The followed Boltzmann transport calculation confirms that HCNs exhibit high Seebeck coefficient and high power factor by appropriate doping. On the other hand, the NEMD simulations show that the phonon induced thermal conductivities of HCNs are almost one order of magnitude smaller than those of CNTs due to the strong tube–tube interaction. Consequently, the thermoelectric properties of HCNs are much higher than those of the corresponding individual CNTs. Within the relaxation time approximation, the maximum *ZT* value of HCN (9,0) may reach 0.8 at 900 K and can be further enhanced with a further reduced lattice thermal conductivity. Our theoretical work suggests that three-dimensional HCNs are more feasible to be applied as thermoelectric devices than individual HCNs or disordered CNT bulk materials.

Acknowledgements

This work was supported by the National Natural Science Foundation of China (11404350, 11404348 and 11204326), China Postdoctoral Science Foundation (2014M551782), Zhejiang Province Preferential Postdoctoral Funded Project (BSH1402077 and BSH1402080), and Ningbo Municipal Natural Science Foundation (2014A610003 and 2014A610008). All the calculations were performed in the PC Cluster from Sugon Company of China.

References

1 G. A. Slack, in *CRC Handbook of Thermoelectrics*, ed. D. M. Rowe, CRC Press, Boca Raton FL, 1995, p. 407.
2 A. Bejan, and A. D. Allan, in *Heat Transfer Handbook*, Wiley, New York, 2003, p. 1338.

3 S. Berber, Y. K. Kwon and D. Tonánek, *Phys. Rev. Lett.*, 2000, **84**, 4613.
4 C. Yu, L. Shi, Z. Yao, D. Li and A. Majumdar, *Nano Lett.*, 2005, **5**, 1842.
5 E. Pop, D. Mann, J. Cao, Q. Wang, K. Goodson and H. Dai, *Phys. Rev. Lett.*, 2005, **95**, 155505.
6 Y. Gu and Y. Chen, *Phys. Rev. B: Condens. Matter Mater. Phys.*, 2007, **76**, 134110.
7 M. S. Dresselhaus, G. Dresselhaus and A. Jorio, *Annu. Rev. Mater. Res.*, 2004, **34**, 247.
8 J. W. Jiang, J. S. Wang and B. Li, *J. Appl. Phys.*, 2011, **109**, 014326.
9 H. L. Zhang, J. F. Li, K. F. Yao and L. D. Chen, *J. Appl. Phys.*, 2005, **97**, 114310.
10 R. S. Prasher, X. J. Hu, Y. Chalopin, N. Mingo, K. Lofgreen, S. Volz, F. Cleri and P. Keblinski, *Phys. Rev. Lett.*, 2009, **102**, 105901.
11 J. Chen, X. Gui, Z. Wang, Z. Li, R. Xiang, K. Wang, D. Wu, X. Xia, Y. Zhou, Q. Wang, Z. Tang and L. Chen, *ACS Appl. Mater. Interfaces*, 2012, **4**, 81.
12 C. Meng, C. Liu and S. Fan, *Adv. Mater.*, 2010, **22**, 535.
13 D. Kim, Y. Kim, K. Choi, J. C. Grunlan and C. Yu, *ACS Nano*, 2010, **4**, 513.
14 Y. W. Wen, X. Liu, X. Duan, K. Cho, R. Chen and B. Shan, *J. Phys. Chem. C*, 2013, **117**, 4951.
15 G. Kresse and J. Hafner, *Phys. Rev. B: Condens. Matter Mater. Phys.*, 1993, **47**, R558.
16 G. Kresse and J. Hafner, *Phys. Rev. B: Condens. Matter Mater. Phys.*, 1994, **49**, 14251.
17 G. Kresse and J. Furthmüller, *Comput. Mater. Sci.*, 1996, **6**, 15.
18 J. P. Perdew, K. Burke and M. Ernzerhof, *Phys. Rev. Lett.*, 1996, **77**, 3865.
19 G. K. H. Madsen and D. J. Singh, *Comput. Phys. Commun.*, 2006, **67**, 175.
20 D. J. Singh, *Sci. Adv. Mater.*, 1996, **3**, 561.
21 S. Plimpton, *J. Comput. Phys.*, 1995, **117**, 1.
22 J. Tersoff, *Phys. Rev. B: Condens. Matter Mater. Phys.*, 1989, **39**, 5566.
23 F. Müller-Plathe, *Phys. Rev. E: Stat. Phys., Plasmas, Fluids, Relat. Interdiscip. Top.*, 1999, **59**, 4894.
24 Y. Z. Pei, X. Y. Shi, A. LaLonde, H. Wang, L. D. Chen and G. J. Suyner, *Nature*, 2011, **473**, 66.
25 M. G. Holland, *Phys. Rev.*, 1963, **132**, 2461.
26 M. B. Nardelli, *Phys. Rev. B: Condens. Matter Mater. Phys.*, 1999, **60**, 7828.
27 S. Datta, *Superlattices Microstruct.*, 2000, **28**, 253.
28 X. J. Tan, H. J. Liu, Y. W. Wen, H. Y. Lv, L. Pan, J. Shi and X. F. Tang, *Nanoscale Res. Lett.*, 2012, **7**, 116.
29 P. K. Schelling, S. R. Phillpot and P. Keblinski, *Phys. Rev. B: Condens. Matter Mater. Phys.*, 2002, **65**, 144306.
30 C. W. Chang, D. Okawa, H. Garcia, A. Majumdar and A. Zettl, *Phys. Rev. Lett.*, 2008, **101**, 075903.
31 J. X. Cao, X. H. Yan, Y. Xiao and J. W. Ding, *Phys. Rev. B: Condens. Matter Mater. Phys.*, 2004, **69**, 073407.
32 G. D. Mahan, in *Thermoelectrics Handbook: Macro to Nano*, CRC press, New York, 2005, chap. 17.
33 W. J. Liang, M. Bockrath and H. Park, *Annu. Rev. Phys. Chem.*, 2005, **56**, 475.
34 J.-C. Charlier, X. Blase and S. Roche, *Rev. Mod. Phys.*, 2007, **79**, 677.
35 M. S. Purewal, B. H. Hong, A. Ravi, B. Chandra, J. Hone and P. Kim, *Phys. Rev. Lett.*, 2007, **98**, 186808.
36 N. Yang, G. Zhang and B. Li, *Nano Lett.*, 2008, **8**, 276.
37 T. Markussen, A.-P. Jauho and M. Brandbyge, *Phys. Rev. Lett.*, 2009, **103**, 055502.